

Channelrhodopsin-2–assisted circuit mapping of long-range callosal projections

Leopoldo Petreanu, Daniel Huber, Aleksander Sobczyk & Karel Svoboda

The functions of cortical areas depend on their inputs and outputs, but the detailed circuits made by long-range projections are unknown. We show that the light-gated channelrhodopsin-2 (ChR2) is delivered to axons in pyramidal neurons *in vivo*. In brain slices from ChR2-expressing mice, photostimulation of ChR2-positive axons can be transduced reliably into single action potentials. Combining photostimulation with whole-cell recordings of synaptic currents makes it possible to map circuits between presynaptic neurons, defined by ChR2 expression, and postsynaptic neurons, defined by targeted patching. We applied this technique, ChR2-assisted circuit mapping (CRACM), to map long-range callosal projections from layer (L) 2/3 of the somatosensory cortex. L2/3 axons connect with neurons in L5, L2/3 and L6, but not L4, in both ipsilateral and contralateral cortex. In both hemispheres the L2/3-to-L5 projection is stronger than the L2/3-to-L2/3 projection. Our results suggest that laminar specificity may be identical for local and long-range cortical projections.

The cortical wiring diagram, consisting of local columnar and laminar microcircuits and their inputs and outputs, underlies neocortical function and plasticity. Neocortical microcircuits are thought to be highly stereotyped and similar across functionally distinct cortical areas¹. The function of cortical areas is largely defined by their inputs and outputs. An important challenge in neuroanatomy is therefore the description of the precise synaptic connectivity of the long-range projections that couple neurons in different brain regions.

Most existing knowledge about the cortical wiring diagram is derived from reconstructions of axonal and dendritic arbors (neurogeometry)^{2–5}. The underlying principle is that connections occur where axons and dendrites overlap. By definition, neurogeometry does not account for specificity beyond the shapes of axons and dendrites and does not predict the strengths of functional connections⁵.

Recordings from pairs of neurons in brain slices provide detailed information about the synapses between connected neurons and can be used to estimate connection probabilities^{6–9}. But this technique is slow and inefficient, and it has only been used to analyze experimentally favorable subcolumnar circuits. The strengths of connections between

positionally defined groups of neurons can be measured by combining laser scanning photostimulation (LSPS) with glutamate uncaging and whole-cell recording^{5,10,11}. However, LSPS with glutamate uncaging indiscriminately stimulates all neurons expressing glutamate receptors and can only probe the small subset of local projections that are preserved in brain slices.

The shortcomings of LSPS with glutamate uncaging could potentially be overcome by replacing uncaging of glutamate with photoactivation of genetically encoded photosensitivity^{12–19}. We therefore developed channelrhodopsin-2 (ChR2)¹⁴ assisted circuit mapping (CRACM), an efficient method to dissect local and long-range synaptic circuits in brain slices. CRACM maps connections between presynaptic ChR2-positive neurons and postsynaptic neurons that are targeted by whole-cell recordings. Because ChR2-positive axons can be photostimulated even if they are severed from their parent somata, CRACM can be used to map circuits that are not preserved in brain slices. We used CRACM to study long-range callosal projections that connect cortical hemispheres.

RESULTS

ChR2-mediated photoexcitation of L2/3 pyramidal neurons

CRACM is based on LSPS and ChR2, a directly light-gated cation channel with rapid kinetics²⁰. Neurons expressing ChR2 can fire action potentials when excited with flashes of blue light^{15–19}. We used *in utero* electroporation²¹ to deliver ChR2-Venus together with mCherry²² to layer (L) 2/3 pyramidal neurons in a region including the right barrel cortex in mice (Methods). Coronal brain slices (**Fig. 1a**) prepared from postnatal day (P) 30 mice contained neurons expressing mCherry (**Fig. 1b**) and ChR2-Venus (**Fig. 1c,d**). Under our conditions the vast majority of transfected cells were L2/3 pyramidal neurons (>99.4%, $n = 4,864$, 4 animals)²³. Labeled axons ramified in L2/3 and L5 and continued into the white matter and the corpus callosum (**Fig. 1c**).

We characterized the excitability of ChR2-positive neurons in brain slices. Brief (1 ms) pulses of blue (473 nm) laser light (50 μ W) applied to the soma elicited inward currents (>100 pA) with rapid kinetics (**Fig. 1e**)^{15–18}. Notably, addition of retinal to the extracellular medium was not necessary, indicating that the level of endogenous retinal in a brain slice is sufficient to make ChR2 functional^{16,17,24}. Repetitive photostimulation caused desensitization of ChR2, which recovered

Howard Hughes Medical Institute, Janelia Farm Research Campus, 19700 Helix Drive, Ashburn, Virginia 20147, USA, and Cold Spring Harbor Laboratory, 1 Bungtown Rd., Cold Spring Harbor, New York 11724, USA. Correspondence should be addressed to K.S. (svobodak@janelia.hhmi.org).

Received 8 November 2006; accepted 12 March 2007; published online 15 April 2007; doi:10.1038/nn1891

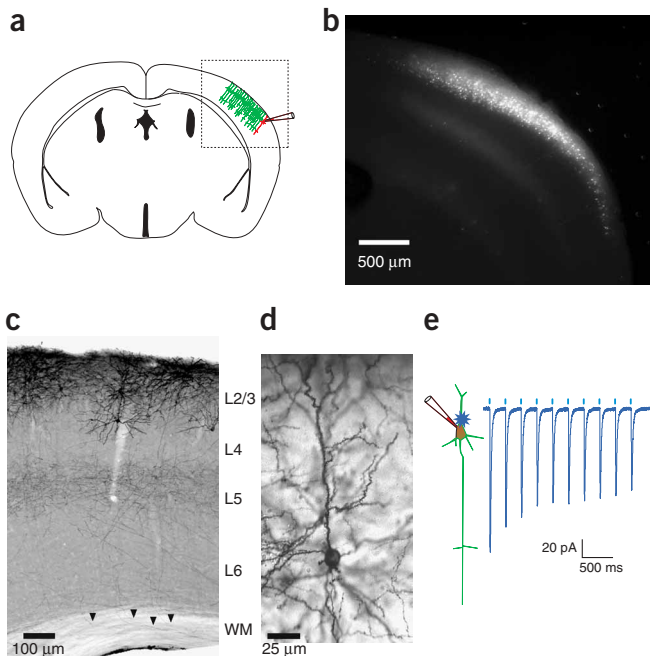


Figure 1 Photostimulation of ChR2-positive neocortical L2/3 pyramidal neurons. (a) Schematic showing the electroporation and recording geometry. The box indicates the approximate location of the image in b. (b) mCherry fluorescence in a coronal slice of the electroporated hemisphere. (c) Immunostaining of ChR2-Venus-expressing cells in the neocortex. Axons enter the white matter (WM, arrowheads) on their way to the corpus callosum. (d) High-resolution image showing an individual L2/3 neuron. (e) Whole-cell voltage-clamp recording from a ChR2-positive L2/3 cell. Light stimuli (1-ms duration) are indicated by blue ticks at top.

after 30 s of rest (Figs. 1e and Supplementary Fig. 1 online)¹⁸. Different ChR2-positive cells responded with different current amplitudes, reflecting varying levels of ChR2 expression among electroporated cells (Supplementary Fig. 1).

Photostimulation of ChR2-positive axons

To analyze the coupling between photostimulation and action potential generation, we recorded somatic membrane potentials in the presence of glutamate receptor blockers (3-(R)-2-carboxypiperazin-4-propyl-1-phosphonic acid (CPP), 5 μM; 2,3-dioxo-6-nitro-1,2,3,4-tetrahydro-benzo[f]quinoxaline-7-sulfonamide, 10 μM). We used LSPS to stimulate the entire depth of the cortex (8 × 16 grid, spacing 75 μm) (Fig. 2a). Stimulation on the soma and dendrites depolarized the cell and in some hot spots triggered action potentials. Cells could also be driven to spike when the laser was directed onto the descending axon, far from the soma

and dendrites. When the stimulus was on the axon in L5, the light caused action potentials without prior depolarization (Fig. 2b), confirming that action potentials were initiated electrotonically distant from the somatic recording pipette. Neurons could also be driven by stimulating the axon in L2/3, L4 and L6 (Supplementary Fig. 2 online). The widths of action potentials evoked by photostimulation and current injections were indistinguishable (width at half maximum from threshold: current injection, 2.4 ± 0.56 ms, n = 9; photostimulation, 2.2 ± 0.19 ms, n = 6). The delay between light pulse and action potential was small (Fig. 2c), (7.7 ± 1.9 ms; range, 3.5–11 ms), with little trial-to-trial jitter (~1 ms) (Fig. 2b inset, Fig. 2c and Supplementary Fig. 1).

With increasing light intensity, axons switched suddenly from firing no action potentials to firing action potentials with probability 1 (Fig. 2d). Although the minimal power at which action potentials could be elicited differed from cell to cell, for an individual cell the transition from probability 0 to 1 occurred over a narrow range in power levels (~10%) (Fig. 2e). Identical light intensities often evoked action potentials in the somata and in dendritic and axonal hot spots. Axonal photostimulation reliably induced action potentials at frequencies up to 8 Hz, and in some cells up to 24 Hz (Supplementary Fig. 1). The spike delay decreased with increasing laser powers (Fig. 2f).

ChR2-assisted circuit mapping

Our experiments show that ChR2 is transported into axons where it can efficiently transduce photostimulation into action potentials. Because axons can be stimulated even if they are severed from their parent somata, CRACM could provide a method to study long-range connections in brain slice preparations. We thus applied CRACM to the study of callosal projections to the somatosensory cortex. The corpus callosum is critical for fusing percepts generated separately in the two

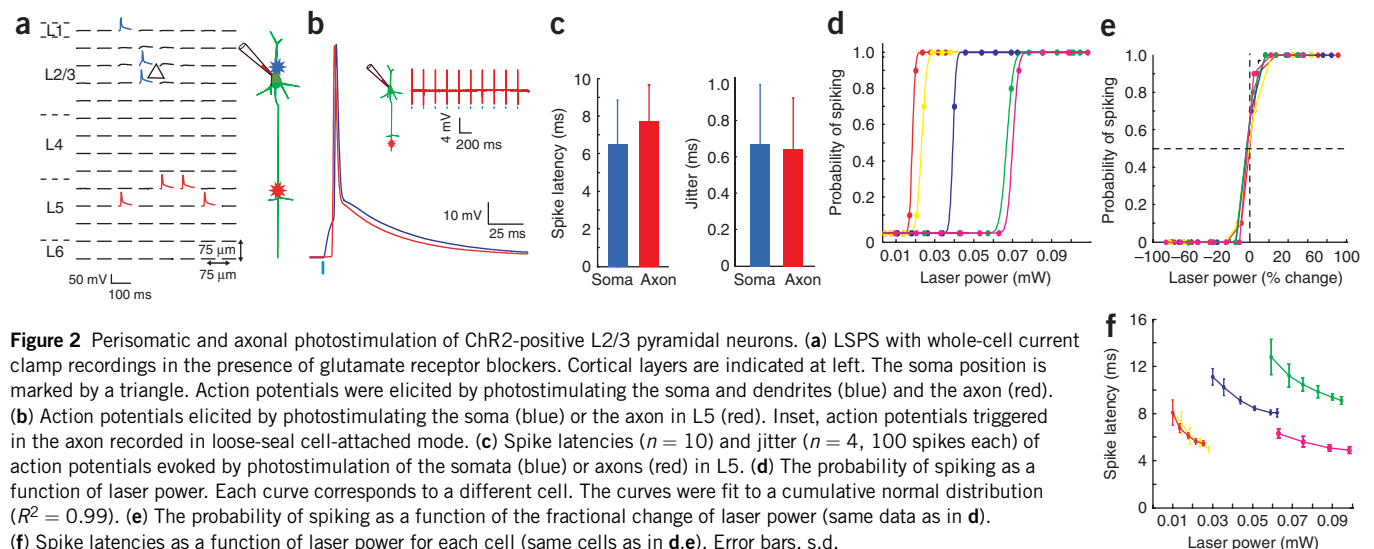


Figure 2 Perisomatic and axonal photostimulation of ChR2-positive L2/3 pyramidal neurons. (a) LSPS with whole-cell current clamp recordings in the presence of glutamate receptor blockers. Cortical layers are indicated at left. The soma position is marked by a triangle. Action potentials were elicited by photostimulating the soma and dendrites (blue) and the axon (red). (b) Action potentials elicited by photostimulating the soma (blue) or the axon in L5 (red). Inset, action potentials triggered in the axon recorded in loose-seal cell-attached mode. (c) Spike latencies (n = 10) and jitter (n = 4, 100 spikes each) of action potentials evoked by photostimulation of the somata (blue) or axons (red) in L5. (d) The probability of spiking as a function of laser power. Each curve corresponds to a different cell. The curves were fit to a cumulative normal distribution (R² = 0.99). (e) The probability of spiking as a function of the fractional change of laser power (same data as in d). (f) Spike latencies as a function of laser power for each cell (same cells as in d,e). Error bars, s.d.

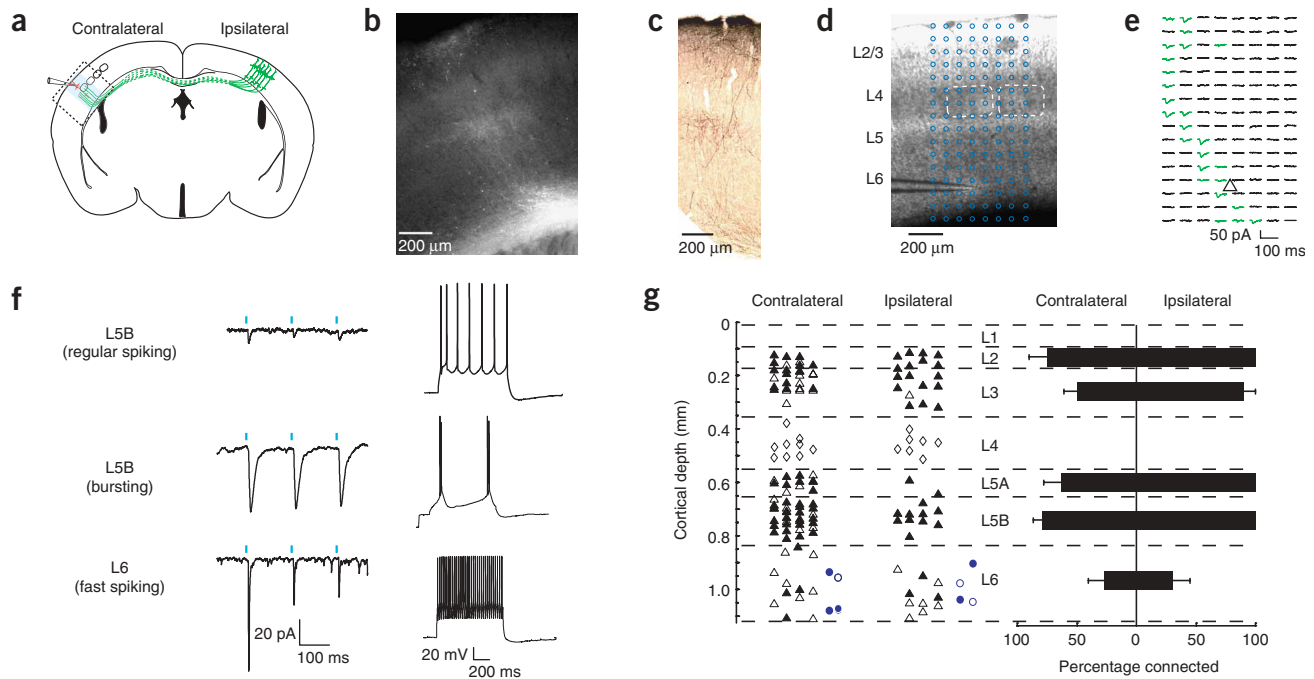


Figure 3 Analysis of the synaptic targets of L2/3 pyramidal cells in the contralateral and ipsilateral barrel cortex. (a) Schematic showing the electroporation and recording geometry. Recording and photostimulation were either in the ipsilateral (electroporated) or the contralateral side. The dashed box indicates the location of the image in b. The blue rectangle indicates the approximate location of the LSPS maps as shown in d,e. (b) mCherry fluorescence of L2/3 axons in the barrel cortex contralateral to the electroporation. (c) Immunohistochemistry of ChR2-Venus showing ascending axons in the contralateral hemisphere. (d) Bright-field image of a barrel cortex slice showing the recording pipette and the photostimulation locations (blue dots; corresponding to e). The positions of barrels are indicated by the dashed white boxes (the barrel in the center of the map corresponds to mouse whisker row 'A'). (e) LSPS map for an L6 cell receiving L2/3 inputs from the contralateral hemisphere. Traces with EPSCs are in green (triangle indicates position of the recorded soma). (f) Examples of EPSCs evoked by photostimulation of ChR2-positive axons in the contralateral hemisphere. Right, spiking patterns. (g) Left, laminar positions of recorded cells ipsilateral or contralateral to the electroporated hemisphere. Solid symbols indicate cells showing EPSCs in response to photostimulation of ChR2-positive axons and open symbols indicate cells that did not show EPSCs. Triangles, pyramidal cells; diamonds, stellate cells; blue circles, fast-spiking interneurons. Right, the fraction of stellate and pyramidal cells receiving input from L2/3 cells. Error bars, binomial standard errors.

cortical hemispheres²⁵. Callosum-projecting neurons originate from pyramidal cells in all cortical layers, but mostly in L3 and L5 (refs. 26,27). This commissural projection terminates in homotopic and heterotopic areas in the contralateral cortex²⁶. The postsynaptic targets of L2/3 axons in the contralateral cortex are unknown.

To identify these targets, we analyzed cortical cells from the left hemisphere, contralateral to the electroporated side (Fig. 3a). mCherry-labeled axons crossed the midline through the corpus callosum and arborized in the contralateral somatosensory cortex. Consistent with previous studies, labeled axons were sparse in most of the contralateral barrel cortex^{26,28}. However, dense bundles of mCherry-positive axons ascended along the edges of the most lateral barrels, which represent whisker row 'A' of the mouse (Fig. 3b–d)²⁸. These axons traversed all cortical layers and arborized in L5, L2/3 and L1 (Fig. 3b,c).

We made whole-cell recordings from neurons in the left barrel cortex containing labeled axons (these axons were severed from their parent somata in the right hemisphere) (Fig. 3a). Neurons were targeted in different cortical layers (3–15 cells per slice). We used LSPS to photostimulate an area encompassing the recorded neuron's entire home cortical column and adjacent areas (area, 0.6 × 1.2 mm) (Fig. 3d). In a subset of LSPS locations, photostimulation elicited reliable excitatory postsynaptic currents (EPSCs) in the recorded cells (Fig. 3e,f). These currents were most likely monosynaptic, for the following reasons. (i) EPSCs had short latencies (6.75 ± 1.92 ms,

range 3.4–11.6 ms, *n* = 43), with little temporal jitter (0.59 ± 0.34 ms, *n* = 22), similar to spike latencies (Fig. 2c). (ii) If responses were multisynaptic in some layers, then the latencies of the EPSCs would differ between layers. However, EPSC latencies were not distinguishable across layers (L2, 6.9 ± 1.9 ms; L3, 7.6 ± 2 ms; L5A, 6.3 ± 2 ms; L5B, 6.5 ± 1.6 ms; L6, 7.15 ± 3 ms; *P* > 0.7, ANOVA). (iii) Cells recorded in current clamp did not generate action potentials (*n* = 23, amplitude of EPSPs 2.55 ± 1.77 mV). Hot spots of excitation often seemed to follow the trajectories of individual axons (Fig. 3d,e). In some places, however, EPSCs were most likely the result of photostimulating more than one axon (Supplementary Fig. 3 online). As a result, a subset of EPSCs contained notches in their rising phase, reflecting the temporal summation of slightly desynchronized EPSCs (Supplementary Fig. 3).

We detected EPSCs in excitatory neurons in L2, L3, L5A, L5B and L6 but never in L4 (Fig. 3f,g). Connections to L5 and L2/3 cells were abundant, whereas connections to L6 cells were relatively rare (Fig. 3g) (*P* < 0.02, *z*-test). L2/3 axons did not distinguish between intrinsically bursting and regular spiking cells in L5B²⁹. A subpopulation of fast-spiking interneurons in L6 also received callosal input from L2/3 (4/5 neurons)³⁰ (Fig. 3f,g).

Thus L2/3 callosal axons connect to pyramidal cells in L5, L2/3 and L6 (in the order of decreasing abundance of connections), but not to neurons in L4. We also analyzed the targets of L2/3 axons in the electroporated (right) hemisphere. Consistent with previous work,

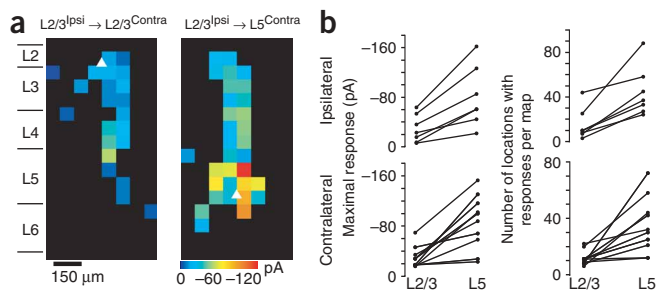


Figure 4 Comparison of L2/3-to-L2/3 and L2/3-to-L5 projections. (a) LSPS maps of L2/3 inputs to a L2/3 cell (left) and a L5 cell (right). Both cells were in the same cortical column (contralateral to the electroporated hemisphere) and the maps were acquired at the same laser power. The color code represents the EPSC amplitude (white triangle indicates the position of the soma). (b) L2/3-to-L5 projections are stronger than L2/3-to-L2/3 projections. Left, maximal response per map. Right, number of pixels per LSPS map that elicited a response. Pairs of L2/3 and L5 cells recorded in the same column are connected by a line.

L2/3 axons made synapses with L2, L3, L5 and a subset of L6 pyramidal neurons in their home column^{8,31} (Fig. 3g). Therefore, the patterns of connections made by L2/3 neurons were very similar in the ipsilateral and contralateral cortex.

We next examined the relative strengths of L2/3-to-L5 and L2/3-to-L2/3 projections. For these experiments we compared postsynaptic L2/3 and L5 neurons in the same brain slice and cortical column using identical stimuli. If we assume that the same axons project to L2/3 and L5, then a relative measure of the number of connected axons is given by the number of photostimulation locations that evoke EPSCs. The numbers of laser positions that elicited EPSCs were larger for postsynaptic L5 than L2/3 cells in both hemispheres (ipsilateral, $P < 0.004$; contralateral, $P < 0.007$, paired t -test) (Fig. 4). Similarly, the amplitudes of the maximal recorded EPSC, which is proportional to the number of connected axons times the amplitude of the unitary EPSC, were larger for postsynaptic L5B than L2/3 cells (ipsilateral, $P < 0.004$; contralateral, $P < 0.003$, paired t -test) (Fig. 4b). This indicates that the L2/3-to-L5 projection is stronger than the L2/3-to-L2/3 projection in both hemispheres.

DISCUSSION

We have used CRACM to dissect the laminar specificity of long-range callosal projections. Long-range projections, including callosal axons, have previously been studied using electrical stimulation^{30,32,33} and electron microscopy^{30,34,35}. In these previous studies callosal axons originating from different layers could not be distinguished. Unlike electrical stimulation, photostimulation is specific to ChR2-positive presynaptic elements, allowing the study of genetically defined neuronal populations. For example, we were able to specifically photostimulate L2/3 callosal axons, sparing other axons that share the same axonal tract. The reliability and low temporal jitter of photostimulation of ChR2 positive axons and somata offers the opportunity to combine circuit mapping with quantitative analysis of synaptic properties. For example, it is possible to study short-term plasticity between defined neuronal populations (Fig. 3f). Similarly, the induction of long-term potentiation should be feasible. In addition, the photostimulation intensity can be tuned to excite a variable number of axons (Supplementary Fig. 3); stimulation of one axon will allow the measurement of the strengths and properties of unitary synaptic connections³⁶. Other methods providing genetically encoded light sensitivity could be used for similar types of circuit analysis^{12,13}.

Using CRACM we confirmed that L2/3 pyramidal neurons connect to pyramidal cells in L2, L3, L5 (ref. 8) and a subset of L6 cells³¹ in their home column (ipsilateral hemisphere). Notably, we found that L2/3 axons contact the same subset of excitatory neurons in the contralateral hemisphere. Supragranular callosal projections are known to originate mostly from L3, with a minor contribution from L2 (refs. 26,27). It is therefore likely that most of the photostimulated callosal axons originated in L3. In the ipsilateral hemisphere, CRACM cannot distinguish between L2 and L3 axons, because both L2 and L3 cells are labeled with our gene delivery method and have abundant local collaterals. L3 cells are known to connect with L2, L3 and L5 cells in their home column^{8,37}, however, confirming our supposition that local and callosal projections from L3 have the same laminar specificity.

The development of cortical circuits is guided by genetic and activity-dependent mechanisms³⁸. Local³⁹ and callosal⁴⁰ L2/3 axons develop with an initial phase of exuberant growth, followed by experience-dependent pruning. Local circuits with laminar specificity made by L2/3 axons were detected as early as postnatal day 14, whereas callosal circuits were first detectable only 1 week later (data not shown). Therefore local and callosal axons are shaped by distinct patterns of activity during different phases of development. In addition, local axons descend from the upper layers into the white matter, whereas callosal axons ascend from the white matter toward L1. This implies that the molecular gradients encountered by local and callosal axons also differ. The laminar targeting of L2/3 axons is therefore likely to be determined by the molecular identity of the postsynaptic neurons, rather than by patterns of activity⁴¹ or diffusible gradients⁴².

METHODS

In utero electroporation. All experimental protocols were conducted according to the US National Institutes of Health guidelines for animal research and were approved by the Institutional Animal Care and Use Committee at the Cold Spring Harbor Laboratory and Janelia Farm Research Campus. Venus⁴³ (gift from A. Miyawaki) was fused to the C terminus of the first 315 amino acids of channelrhodopsin-2 (gift from G. Nagel). The constructs were inserted into pCAGGS vector modified for *in utero* electroporation⁴⁴. DNA was purified and concentrated using Qiagen plasmid preparation kits and dissolved in 10 mM Tris-HCl (pH 8.0).

L2/3 progenitor cells were transfected via *in utero* electroporation²¹. Embryonic day 16 timed-pregnant C57BL/6J mice (Charles River) were deeply anesthetized using an isoflurane-oxygen mixture (1% (vol/vol) isoflurane in O₂) delivered by an anesthesia regulator (SurgiVet). The uterine horns were exposed and ~1 μl of DNA solution with Fast Green (Sigma) was pressure injected (Picospritzer, General Valve) through a pulled glass capillary tube (Warner Instruments) into the right lateral ventricle of each embryo. The DNA solution contained a mixture of plasmids encoding ChR2-Venus and mCherry in a 3:1 molar ratio, at final concentration of 2 μg μl⁻¹. In animals used for immunohistochemistry, the mCherry plasmid was omitted from the mixture. The head of each embryo was placed between custom-made tweezer electrodes, with the positive plate contacting the right side of the head. Electroporation was achieved with five square pulses (duration 50 ms, frequency 1 Hz, 40 V). mCherry fluorescence was used to screen for positive animals under a fluorescent dissecting scope (MVX10, Olympus), 1–2 d after birth. It also allowed us to search for fluorescent cells and axons on brain slices during the experiment without depolarizing the ChR2-positive cells.

The transfected cortical region in electroporated animals was always restricted to L2/3 in the electroporated hemisphere. It usually encompassed most of the barrel cortex and in some cases included parts of auditory, visual and secondary somatosensory areas.

Slice preparation. P30–P35 mice were used in these experiments. In younger animals it was difficult to elicit synaptic responses by photostimulating callosal axons. Animals were anesthetized with an intraperitoneal injection of



a ketamine-xylazine mixture (0.13 mg ketamine and 0.01 mg xylazine per g body weight) and perfused through the heart with a small volume of ice-cold ACSF containing 127 mM NaCl, 25 mM NaHCO₃, 25 mM D-glucose, 2.5 mM KCl, 1 mM MgCl₂, 2 mM CaCl₂ and 1.25 mM NaH₂PO₄, aerated with 95% O₂/5% CO₂. The brain was removed and placed in an ice-cold cutting solution containing 110 mM choline chloride, 25 mM NaHCO₃, 25 mM D-glucose, 11.6 mM sodium ascorbate, 7 mM MgCl₂, 3.1 mM sodium pyruvate, 2.5 mM KCl, 1.25 mM NaH₂PO₄ and 0.5 mM CaCl₂. 300- μ m-thick coronal slices of the barrel cortex were cut with a vibrating slicer (Microm) and incubated in oxygenated ACSF for 45 min at 37 °C before the recordings.

Electrophysiology and photostimulation. Recordings were performed at room temperature (22–24 °C). Brain slices were screened for electroporated neurons using a custom filter set that allowed us to detect mCherry fluorescence while minimizing ChR2 activation (excitation, 550–600 nm; emission, 610 nm long pass; Chroma). Neurons were visualized under infrared differential interference optics and patched with borosilicate pipettes (resistance 4–6 M Ω). The intracellular solution contained 120 mM potassium gluconate, 5 mM NaCl, 2 mM MgCl₂, 0.1 mM CaCl₂, 10 mM HEPES, 1.1 mM EGTA, 4 mM magnesium ATP, 0.4 mM disodium GTP, 15 mM sodium phosphocreatine and 0.015 mM Alexa-594 (Molecular Probes) (pH 7.25; 290 mOsm). Cells were recorded at a depth of 50–95 μ m in the brain slice. For photostimulation we used a blue laser (473 nm; Crystal Laser) delivered through an air immersion objective (4 \times ; 0.16 NA; UPlanApo, Olympus). Stimulation was with a beam diameter of \sim 5–10 μ m (scattering in the tissue was not taken into account). Photostimuli consisted of light pulses with 1-ms durations and powers in the range 25–500 μ W at the specimen. Repeated photostimulation did not elicit responses in ChR2-negative cells (**Supplementary Fig. 4** online). Even prolonged exposure with blue light did not induce damage (**Supplementary Fig. 4**). The duration and intensity of the light pulses were controlled with a Pockels cell (ConOptics) and a shutter (Uniblitz) and custom software written in Matlab (Mathworks).

Characterizing the excitation of ChR2-positive neurons was performed in the presence of blockers of glutamate receptors (CPP, 5 μ M; NBQX, 10 μ M). EPSCs were recorded in voltage clamp (–70 mV) (**3e,f**). Spikes were recorded in whole-cell current clamp (**Fig. 2a,b**) or in loose-seal cell-attached mode (**Figs. 2b**, inset, and **Supplementary Fig. 1**). To measure the spiking probability and latency at different laser powers (**Fig. 2d–f**), a power series (ten powers) was delivered with ten repetitions (interstimulus interval, 30 s).

For CRACM we delivered three light pulses (interpulse interval 150 ms) every 700 ms (**Fig. 3d–f**) on a 8 \times 16 grid. The grid area (0.6 \times 1.2 mm²) included the entire thickness of the cortical gray matter. Stimulation with trains of pulses allowed us to distinguish photostimulation-evoked responses from spontaneous synaptic activity. Stimuli were given in a spatial sequence designed to maximize the time between stimuli to neighboring spots⁴⁵. Laser power ranged from 25 μ W to 100 μ W for the electroporated hemisphere and 150 μ W to 500 μ W in the contralateral hemisphere. In calculating the percentage of connected cell (**Fig. 3g**), cells were included only if at least one cell in the cortical column displayed photostimulation-evoked EPSCs. Even with relatively high photostimulation powers, the response probability was substantially larger in the ipsilateral cortex than in the contralateral cortex (**Fig. 3g**), presumably reflecting the higher density of ChR2 axons in the ipsilateral cortex. During recording of cells in the same cortical columns (**Fig. 4**), laser power and photostimulation locations were kept constant across cells. This allowed us to measure relative connection probabilities and connection strengths for different classes of postsynaptic cells.

Identification and definition of cortical layers. The borders of the cortical layers were defined as follows. L1 was identified by its low cell density. L2/3 was between L1 and the top of the barrels. On the basis of functional mapping studies³⁷, L2 was taken as the top 100 μ m of L2/3. L4 was identified by the presence of barrels in coronal slices. L5A was identified as a white band (under bright-field illumination, **Fig. 3d**) under the barrels (\sim 100 μ m thick). L5B was the layer immediately below L5A, containing large pyramidal cells (\sim 200 μ m

thick). L6 was defined as the layer extending from the bottom of L5B to the white matter.

Immunohistochemistry. ChR2-Venus-electroporated mice were perfused with cold saline and 4% paraformaldehyde (PFA) and fixed overnight in 4% PFA. 60- μ m sections were cut with a vibratome (Leica). Sections were blocked with 0.3% Triton X-100 and 5% goat serum for 6 h at room temperature followed by the antibody to green fluorescent protein (0.1 mg ml^{–1}, 1:700, Chemicon) for 17 h at 4 °C (volume 200 μ l for 24-well plate). Endogenous peroxidases were quenched with 3% H₂O₂ (Fisher) in 0.1 M phosphate buffer, pH 7.4, for 30 min at room temperature. Sections were washed three times for 20 min each time (volume 500 μ l) with Triton X-100 and 5% goat serum and incubated with biotinylated antibody to rabbit (1:200) 16 h at 4 °C; washed three times for 20 min each and incubated in the ABC reaction (Vector) for 2 h at room temperature; and then washed three times for 20 min each and subjected to the diaminobenzidine (DAB) reaction for 5–40 min (prepared fresh each time using 5 ml phosphate buffer, 15 μ l 3% H₂O₂, 100 μ l 1% NiCl and 0.05% DAB). The DAB reaction was stopped with phosphate buffer and washed twice with phosphate buffer and once with water for 10 min each time. Sections were mounted on glass slides, dehydrated with an increasing alcohol series, and coverslipped in DPX mounting medium.

Data in the text are presented as mean \pm s.d. Error bars in charts signify s.d. unless otherwise noted.

Note: Supplementary information is available on the Nature Neuroscience website.

ACKNOWLEDGMENTS

We thank members of our laboratory for discussion, D. Chklovskii, E. Chiappe, G. Shepherd and J. Magee for comments on the manuscript, and T. O'Connor for software development. This work was supported by the Howard Hughes Medical Institute, the US National Institute of Health and the Swiss National Science Foundation (D.H.).

AUTHOR CONTRIBUTIONS

L.P. and K.S. conceived and designed the experiments, analyzed the data and wrote the manuscript. L.P., D.H. and A.S. conducted the experiments. K.S. provided reagents, analysis tools and financial support.

COMPETING INTERESTS STATEMENT

The authors declare no competing financial interests.

Published online at <http://www.nature.com/natureneuroscience>

Reprints and permissions information is available online at <http://npg.nature.com/reprintsandpermissions>

- Douglas, R.J. & Martin, K.A. Neuronal circuits of the neocortex. *Annu. Rev. Neurosci.* **27**, 419–451 (2004).
- Binzegger, T., Douglas, R.J. & Martin, K.A. A quantitative map of the circuit of cat primary visual cortex. *J. Neurosci.* **24**, 8441–8453 (2004).
- Stepanyants, A., Tamas, G. & Chklovskii, D.B. Class-specific features of neuronal wiring. *Neuron* **43**, 251–259 (2004).
- Gilbert, C.D. Microcircuitry of the visual cortex. *Annu. Rev. Neurosci.* **6**, 217–247 (1983).
- Shepherd, G.M.G., Stepanyants, A., Bureau, I., Chklovskii, D.B. & Svoboda, K. Geometric and functional organization of cortical circuits. *Nat. Neurosci.* **8**, 782–790 (2005).
- Gupta, A., Wang, Y. & Markram, H. Organizing principles for a diversity of GABAergic interneurons and synapses in the neocortex. *Science* **287**, 273–278 (2000).
- Thomson, A.M., West, D.C., Wang, Y. & Bannister, A.P. Synaptic connections and small circuits involving excitatory and inhibitory neurons in layers 2–5 of adult rat and cat neocortex: triple intracellular recordings and biocytin labelling in vitro. *Cereb. Cortex* **12**, 936–953 (2002).
- Thomson, A.M. & Bannister, A.P. Interlaminar connections in the neocortex. *Cereb. Cortex* **13**, 5–14 (2003).
- Holmgren, C., Harkany, T., Svennenfors, B. & Zilberter, Y. Pyramidal cell communication within local networks in layer 2/3 of rat neocortex. *J. Physiol. (Lond.)* **551**, 139–153 (2003).
- Katz, L.C. & Dalva, M.B. Scanning laser photostimulation: a new approach for analyzing brain circuits. *J. Neurosci. Methods* **54**, 205–218 (1994).
- Dantzker, J.L. & Callaway, E.M. Laminar sources of synaptic input to cortical inhibitory interneurons and pyramidal neurons. *Nat. Neurosci.* **3**, 701–707 (2000).
- Banghart, M., Borges, K., Isacoff, E., Trauner, D. & Kramer, R.H. Light-activated ion channels for remote control of neuronal firing. *Nat. Neurosci.* **7**, 1381–1386 (2004).
- Zemelman, B.V., Lee, G.A., Ng, M. & Miesenböck, G. Selective photostimulation of genetically chARGed neurons. *Neuron* **33**, 15–22 (2002).

14. Nagel, G. *et al.* Channelrhodopsin-2, a directly light-gated cation-selective membrane channel. *Proc. Natl. Acad. Sci. USA* **100**, 13940–13945 (2003).
15. Boyden, E.S., Zhang, F., Bamberg, E., Nagel, G. & Deisseroth, K. Millisecond-timescale, genetically targeted optical control of neural activity. *Nat. Neurosci.* **8**, 1263–1268 (2005).
16. Li, X. *et al.* Fast noninvasive activation and inhibition of neural and network activity by vertebrate rhodopsin and green algae channelrhodopsin. *Proc. Natl. Acad. Sci. USA* **102**, 17816–17821 (2005).
17. Bi, A. *et al.* Ectopic expression of a microbial-type rhodopsin restores visual responses in mice with photoreceptor degeneration. *Neuron* **50**, 23–33 (2006).
18. Ishizuka, T., Kakuda, M., Araki, R. & Yawo, H. Kinetic evaluation of photosensitivity in genetically engineered neurons expressing green algae light-gated channels. *Neurosci. Res.* **54**, 85–94 (2006).
19. Zhang, Y.P. & Oertner, T.G. Optical induction of synaptic plasticity using a light-sensitive channel. *Nat. Methods* **4**, 139–141 (2006).
20. Nagel, G. *et al.* Channelrhodopsins: directly light-gated cation channels. *Biochem. Soc. Trans.* **33**, 863–866 (2005).
21. Saito, T. & Nakatsuji, N. Efficient gene transfer into the embryonic mouse brain using *in vivo* electroporation. *Dev. Biol.* **240**, 237–246 (2001).
22. Shaner, N.C. *et al.* Improved monomeric red, orange and yellow fluorescent proteins derived from *Discosoma* sp. red fluorescent protein. *Nat. Biotechnol.* **22**, 1567–1572 (2004).
23. Hatanaka, Y., Hisanaga, S., Heizmann, C.W. & Murakami, F. Distinct migratory behavior of early- and late-born neurons derived from the cortical ventricular zone. *J. Comp. Neurol.* **479**, 1–14 (2004).
24. Zhang, F., Wang, L.P., Boyden, E.S. & Deisseroth, K. Channelrhodopsin-2 and optical control of excitable cells. *Nat. Methods* **3**, 785–792 (2006).
25. Gazzaniga, M.S. Forty-five years of split-brain research and still going strong. *Nat. Rev. Neurosci.* **6**, 653–659 (2005).
26. Wise, S.P. & Jones, E.G. The organization and postnatal development of the commissural projection of the rat somatic sensory cortex. *J. Comp. Neurol.* **168**, 313–343 (1976).
27. Ivy, G.O., Akers, R.M. & Killackey, H.P. Differential distribution of callosal projection neurons in the neonatal and adult rat. *Brain Res.* **173**, 532–537 (1979).
28. Olavarria, J., Van Sluyters, R.C. & Killackey, H.P. Evidence for the complementary organization of callosal and thalamic connections within rat somatosensory cortex. *Brain Res.* **291**, 364–368 (1984).
29. Connors, B.W. & Gutnick, M.J. Intrinsic firing patterns of diverse neocortical neurons. *Trends Neurosci.* **13**, 99–104 (1990).
30. Karayannis, T., Huerta-Ocampo, I. & Capogna, M. GABAergic and pyramidal neurons of deep cortical layers directly receive and differently integrate callosal input. *Cereb. Cortex* published online 7 July 2006 (doi:10.1093/cercor/bhl035).
31. Zarrinpar, A. & Callaway, E.M. Local connections to specific types of layer 6 neurons in the rat visual cortex. *J. Neurophysiol.* **95**, 1751–1761 (2006).
32. Vogt, B.A. & Gorman, A.L. Responses of cortical neurons to stimulation of corpus callosum *in vitro*. *J. Neurophysiol.* **48**, 1257–1273 (1982).
33. Kumar, S.S. & Huguenard, J.R. Properties of excitatory synaptic connections mediated by the corpus callosum in the developing rat neocortex. *J. Neurophysiol.* **86**, 2973–2985 (2001).
34. White, E.L. & Czeiger, D. Synapses made by axons of callosal projection neurons in mouse somatosensory cortex: emphasis on intrinsic connections. *J. Comp. Neurol.* **303**, 233–244 (1991).
35. Czeiger, D. & White, E.L. Synapses of extrinsic and intrinsic origin made by callosal projection neurons in mouse visual cortex. *J. Comp. Neurol.* **330**, 502–513 (1993).
36. Raastad, M., Storm, J.F. & Andersen, P. Putative single quantum and single fibre excitatory postsynaptic currents show similar amplitude range and variability in rat hippocampal slices. *Eur. J. Neurosci.* **4**, 113–117 (1992).
37. Bureau, I., von Saint Paul, F. & Svoboda, K. Interdigitated paralemniscal and lemniscal pathways in the mouse barrel cortex. *PLoS Biol.* **4**, e382 (2006).
38. Katz, L.C. & Shatz, C.J. Synaptic activity and the construction of cortical circuits. *Science* **274**, 1133–1138 (1996).
39. Ruthazer, E.S. & Stryker, M.P. The role of activity in the development of long-range horizontal connections in area 17 of the ferret. *J. Neurosci.* **16**, 7253–7269 (1996).
40. Innocenti, G.M. & Price, D.J. Exuberance in the development of cortical networks. *Nat. Rev. Neurosci.* **6**, 955–965 (2005).
41. Dantzker, J.L. & Callaway, E.M. The development of local, layer-specific visual cortical axons in the absence of extrinsic influences and intrinsic activity. *J. Neurosci.* **18**, 4145–4154 (1998).
42. Polleux, F., Morrow, T. & Ghosh, A. Semaphorin 3A is a chemoattractant for cortical apical dendrites. *Nature* **404**, 567–573 (2000).
43. Nagai, T. *et al.* A variant of yellow fluorescent protein with fast and efficient maturation for cell-biological applications. *Nat. Biotechnol.* **20**, 87–90 (2002).
44. Gray, N.W., Weimer, R.M., Bureau, I. & Svoboda, K. Rapid redistribution of synaptic PSD-95 in the neocortex *in vivo*. *PLoS Biol.* **4**, e370 (2006).
45. Shepherd, G.M., Pologruto, T.A. & Svoboda, K. Circuit analysis of experience-dependent plasticity in the developing rat barrel cortex. *Neuron* **38**, 277–289 (2003).

